Inorganic Chemistry

Article

pubs.acs.org/IC

Synthesis, Structures, and Photochemistry of Tricarbonyl Metal Polyoxoanion Complexes, $[X_2W_{20}O_{70}\{M(CO)_3\}_2]^{12-}$ (X = Sb, Bi and M = Re, Mn)

Chongchao Zhao, Choon Sung Kambara, Ye Yang, Alexey L. Kaledin, Djamaladdin G. Musaev, Tianquan Lian, and Craig L. Hill*

Department of Chemistry and Cherry L. Emerson Center for Scientific Computation, Emory University, Atlanta, Georgia 30322, United States

Supporting Information

ABSTRACT: A new series of complexes containing two electron donating groups, $\{M(CO)_3\}^+$ ions, M = Re or Mn, on one polytungstate electron acceptor group have been prepared and characterized. These complexes containing two electron donating groups, $\{M(CO)_3\}^+$ ions, M = Re or Mn, on one polytungstate electron acceptor group have been prepared and characterized. These two-component polyoxometalate (POM) compounds have been made by reaction of solvated $\{M(CO)_3\}^+$ ions (M = Re or Mn) with $[X_2W_{22}O_{74}(OH)_2]^{12-}$ (X = Sb or Bi) POM multidentate ligands in aqueous solution. These syntheses reveal that the *fac*-$\{WO(OH)_2\}^{2+}$ groups in the terminal positions of these two POM ligands are easily replaced by the topologically equivalent units *fac*-$\{M(CO)_3\}^+$. Four compounds, $[X_2W_{20}O_{70}\{M(CO)_3\}_2]^{12-}$ (**1a**: X = Sb, M = Re; **1b**: X = Bi, M = Re; **2a**: X = Sb, M = Mn; **2b**: X = Bi, M = Mn) have been isolated and characterized of X-ray crystallography, spectroscopic, and computational methods. The charge transfer dynamics, investigated by femtosecond transient absorption (TA) spectroscopy of **1a** and **1b** combined with the density functional theory (DFT) calculations indicate that both complexes exhibit metal-to-polyoxometalate charge-transfer (MPCT) from the Re centers to the POM ligands, while MPCT from the Mn centers to the POM ligands in **2a** and **2b** leads to decomposition of starting compounds. The studies suggest a general synthetic route to a potentially very large class of POM-based hybrid compounds.

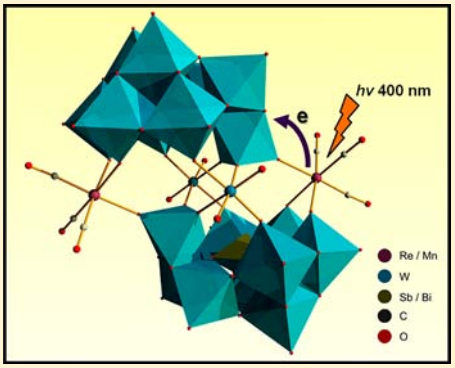

INTRODUCTION

Polyoxometalate (POM)-supported metal carbonyl derivatives have long been studied as tractable, molecular analogues of solid-oxide-supported metal complexes and exhibit an engaging range of properties.[1−3] A series of these hybrid compounds with their preparation strategies, unique structures, and catalytic properties have been reported previously.[4−17] However, most of these compounds involve Lindqvist-type POMs.[4−8] Lacunary POMs (Keggin or Dawson), which tend to form stronger covalent bonds to the incorporated metal multicarbonyl units, have rarely been used as the molecular metal-oxide supports.[14] The photochemical properties and potential value of these complexes in solar fuel production is essentially unstudied. Recently, our group reported a new complex, $[P_4W_{35}O_{124}\{Re(CO)_3\}_2]^{16-}$ (**3**), with a "twisted-sandwich" structure, based on the lacunary ligand, $[\alpha_2\text{-}P_2W_{17}O_{61}]^{10-}$. This compound displays novel intramolecular metal-to-polyoxometalate charge-transfer (MPCT) properties,[18] which in some contexts, is a more robust all-inorganic analogue of (2,2′-bipyridyl)$Re(CO)_3Cl$. The latter complex is both a photosensitizer and catalyst for reducing CO_2 under photochemical and electrochemical conditions.[19−23] Complex **3** has a high absorptivity in the visible region arising from the Re−O−W bond but has a very short excited state lifetime rendering it marginally attractive for application in solar devices. As a result, we sought to investigate multidentate polytungstates with appended metal multicarbonyl donor groups such as $\{M(CO)_3\}^+$ (M = Re or Mn) of other types covalently bound to one POM acceptor unit.

POM-supported metal carbonyl derivatives, which can be regarded as a subcategory of functionalized POMs, are best prepared by stepwise and controlled methods. In this context, the use of appropriate lacunary POMs as chelating ligands is important for directing the reactions toward the desired products.[24−28] Since all these POM-supported metal carbonyl compounds contain a *fac*-$\{M(CO)_3\}^+$ d^6 metal carbonyl fragment, lacunary POMs which can act as tridentate ligands are logical synthetic precursors. Krebs and co-workers prepared and thoroughly characterized tungstoantimonates and tungstobismuthates structurally related to those in this article with the general formula $[X_2W_{20}M_2O_{70}(H_2O)_6]^{(14-2n)-}$ (X = Sb, Bi; M = Fe, Co, Zn).[29,30] In these Krebs dimer complexes, the terminal aqua *fac*-$\{M(H_2O)_3\}^{2+/3+}$ groups replace the *fac*-$\{WO(OH)_2\}^{2+}$ moieties on the POM scaffolds. Appreciating

Received: August 12, 2012
Published: January 3, 2013

   dx.doi.org/10.1021/ic301766b | *Inorg. Chem.* 2013, 52, 671−678

Scheme 1. Representative Strategies for the Preparation of 1a, 1b, 2a, and 2b in Combined Ball-and-Stick and Polyhedral Notations[a]

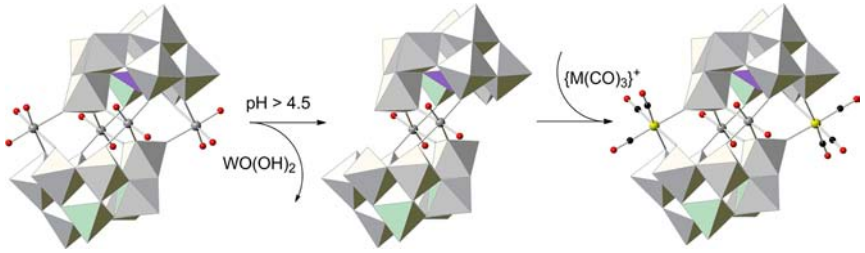

[a]O, red; C, black; W, gray; Sb/Bi, purple; Re/Mn, yellow.

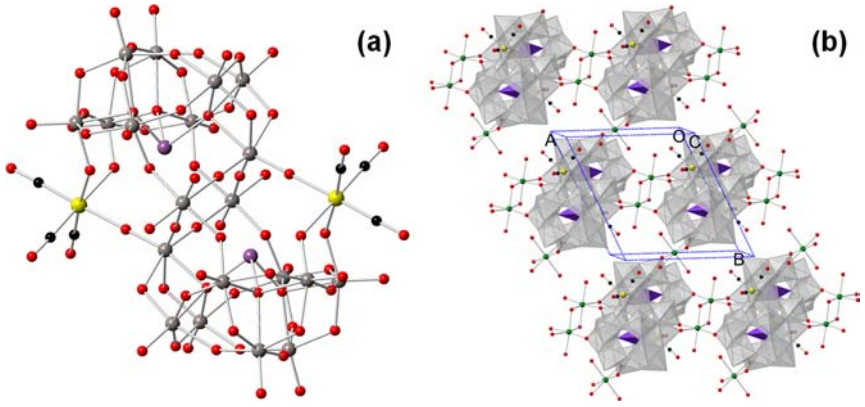

Figure 1. (a) Ball-and-stick representation of **1a**, **1b**, **2a**, and **2b**. Cations K^+, Na^+ and solvent H_2O are omitted for clarity. O, red; C, black; W, gray; Sb/Bi, purple; Re/Mn, yellow. (b) View of the 2D sheet of **1a** in combined ball-and-stick and polyhedral notation. Na, green; O, red; C, black; Re, yellow; WO_6, gray; SbO_3, purple.

that the tricarbonyl *fac*-$\{M(CO)_3\}^+$ unit is also topologically equivalent to *fac*-$\{M(H_2O)_3\}^{2+/3+}$ and *fac*-$\{WO(OH)_2\}^{2+}$, we utilized these POM ligands as multidentate building blocks to coordinate *fac*-$\{M(CO)_3\}^+$ fragments. In this context, we have successfully obtained four Krebs-type "slipped-sandwich" structures: $Na_{11}H[Sb_2W_{20}O_{70}\{Re(CO)_3\}_2]\cdot 34H_2O$ (**1a**), $Na_{11}H[Bi_2W_{20}O_{70}\{Re(CO)_3\}_2]\cdot 33H_2O$ (**1b**), $K_9Na_3[Sb_2W_{20}O_{70}\{Mn(CO)_3\}_2]\cdot 32H_2O$ (**2a**), and $K_9Na_3[Bi_2W_{20}O_{70}\{Mn(CO)_3\}_2]\cdot 32H_2O$ (**2b**). All four compounds have been structurally characterized by single-crystal X-ray diffraction, vibrational and electronic absorption spectroscopy, transient UV−visible spectra, and density functional theory (DFT)/B3LYP calculations (on **1a**).

RESULTS AND DISCUSSION

Synthesis. The natural pH of the POM ligands, $[X_2W_{22}O_{74}(OH)_2]^{12-}$ (X = Sb or Bi), is about 4.5. When the pH increases, two terminal *fac*-$\{WO(OH)_2\}^{2+}$ groups are released from the POM frameworks, and the resulting vacant sites can be occupied by transition metal centers with multiple terminal aqua ligands.[29,30] This assertion is further supported in this paper. The preparation of the four new compounds above is conducted in a weakly acidic aqueous solution (pH 5−6); when pH values are lower than 3, these compounds do not form. The two general steps affording these complexes are illustrated in Scheme 1.

The FTIR spectra of these four compounds are shown in Supporting Information, Figure S1. As expected, **1a** and **1b** share similar patterns in their FTIR spectra as do **2a** and **2b**, but the spectra of the former are slightly distinct from the latter. Since each $\{M(CO)_3\}^+$ moiety has local C_{3v} symmetry and the two $\{M(CO)_3\}^+$ groups are symmetrical, only two symmetric and one antisymmetric IR-active C−O stretching modes are present in the FTIR spectra. This spectral region also reveals the purity of these compounds. As expected, **1a** and **1b** have lower C−O frequencies relative to those in **2a** and **2b**. This is due to stronger M-to-CO $d\pi-\pi^*$ back bonding from Re compared to Mn because Re(I) is more electron donating (and generally has a more negative potential) than Mn(I). The C−O stretching vibrations in **1a** (2016, 1925, 1906 cm^{-1}) and **1b** (2014, 1923, 1901 cm^{-1}) are higher than those in **3** (2006, 1901, 1880 cm^{-1}),[18] which indicates that the POM ligands, $[X_2W_{20}O_{70}]^{14-}$, are stronger electron-acceptors than $[P_4W_{35}O_{124}]^{18-}$ in **3**. Furthermore, the frequencies of the carbonyl bands in **1a** and **1b** are similar to those of $[Re(CO)_3(H_2O)\{Mo_5O_{13}(OMe)_4(NO)\}]^{2-}$ (2013, 1910, 1885 cm^{-1}), but higher than those of $\{[H_2W_8O_{30}][Re(CO)_3]_2\}^{8-}$ (2007, 1885 cm^{-1}).[13,15] In the same context, the frequencies for the manganese carbonyl species follow a similar trend: **2a** has bands at 2031, 1936, 1919 cm^{-1} and **2b** has bands at 2030, 1935, 1919 cm^{-1}, respectively, which are similar to those of $[Mn(CO)_3(H_2O)\{Mo_5O_{13}(OMe)_4(NO)\}]^{2-}$ (2029, 1933, 1916 cm^{-1}) but higher than those in $\{[H_2W_8O_{30}][Mn(CO)_3]_2\}^{8-}$ (2022, 1932 cm^{-1}). These results imply that both $[X_2W_{20}O_{70}]^{14-}$ and $\{Mo_5O_{13}(OMe)_4(NO)\}^{3-}$ have similar electron acceptor strengths and both are stronger acceptors than $[H_2W_8O_{30}]^{10-}$.

Structures. All four metal-donor-POM-acceptor compounds have similar structures and contain two identical *β-B*-$[XW_9O_{33}]^{9-}$ (X = Sb or Bi) units joined by two WO_6 octahedra and two *fac*-$\{M(CO)_3\}^+$ moieties (Figure 1a). The Re and Mn centers exhibit MO_3C_3 coordination octahedra but with slight

dx.doi.org/10.1021/ic301766b | Inorg. Chem. 2013, 52, 671−678

Table 1. Selective Bond Lengths (Å) and Bond Angles (deg) for 1a, 1b, 2a, and 2b

	1a	1a (calcd.)	1b	2a	2b
X−O[a]	2.01−2.02	2.01−2.03	2.13−2.16	1.98−2.00	2.13−2.15
M−O[a]	2.13−2.16	2.16−2.18	2.12−2.15	2.08−2.12	2.06−2.08
M−C[b]	1.87−1.88	1.90	1.85−1.90	1.80−1.90	1.85−1.87
M−C−O[c]	176−179	178−179	177−179	173−177	171−175

[a]Oxygen from the POM frameworks (X = Sb or Bi; M = Re or Mn). [b]Carbon from the carbonyl groups. [c]Oxygen from the carbonyl groups.

Table 2. Crystal Structure Data for Compounds 1a, 1b, 2a, and 2b

	1a	1b	2a	2b
empirical formula	$C_6H_{69}O_{110}Na_{11}Re_2Sb_2W_{20}$	$C_6H_{67}O_{109}Bi_2Na_{11}Re_2W_{20}$	$C_6H_{64}O_{108}Mn_2K_9Na_3Sb_2W_{20}$	$C_6H_{64}O_{110}K_9Na_3Mn_2Bi_2W_{20}$
T [K]	173(2)	173(2)	173(2)	173(2)
M_r [g mol^{-1}]	6447.16	6603.79	6315.55	6521.99
crystal system	triclinic	triclinic	triclinic	triclinic
space group	$P\bar{1}$	$P\bar{1}$	$P\bar{1}$	$P\bar{1}$
a [Å]	13.724(6)	13.672(3)	12.443 (1)	12.446(3)
b [Å]	14.244(6)	14.815(3)	13.095(1)	13.089(3)
c [Å]	17.610(7)	15.385(3)	15.808(1)	15.723(4)
α [deg]	90.315(6)	103.492(3)	83.375 (1)	82.883(4)
β [deg]	107.851(5)	106.042(3)	74.307(1)	73.810(4)
γ [deg]	112.456(6)	104.397(3)	75.043(1)	74.750(3)
V [Å^3]	2999(2)	2743.9(10)	2392.8(3)	2369.7(10)
Z	1	1	1	1
ρ_{calcd} [g cm^{-3}]	3.558	3.897	4.066	4.402
μ [mm^{-1}]	21.691	26.403	25.255	28.642
reflection collected	46970	47376	37914	34752
independent reflections (R_{int})	13181 (0.0829)	13169 (0.0567)	10154 (0.0544)	9310 (0.0611)
goodness-of-fit	1.038	1.037	1.065	1.032
R_1 [$I > 2\sigma(I)$]	0.0575	0.0442	0.0487	0.0584
wR_2	0.1328	0.1213	0.1177	0.1521
R_1 (all data)	0.0873	0.0579	0.0651	0.0764
wR_2	0.1472	0.1307	0.1253	0.1644
largest diff. peak and hole [e Å^3]	4.714, −2.944	3.131, −1.980	3.282, −2.620	8.043, −2.558

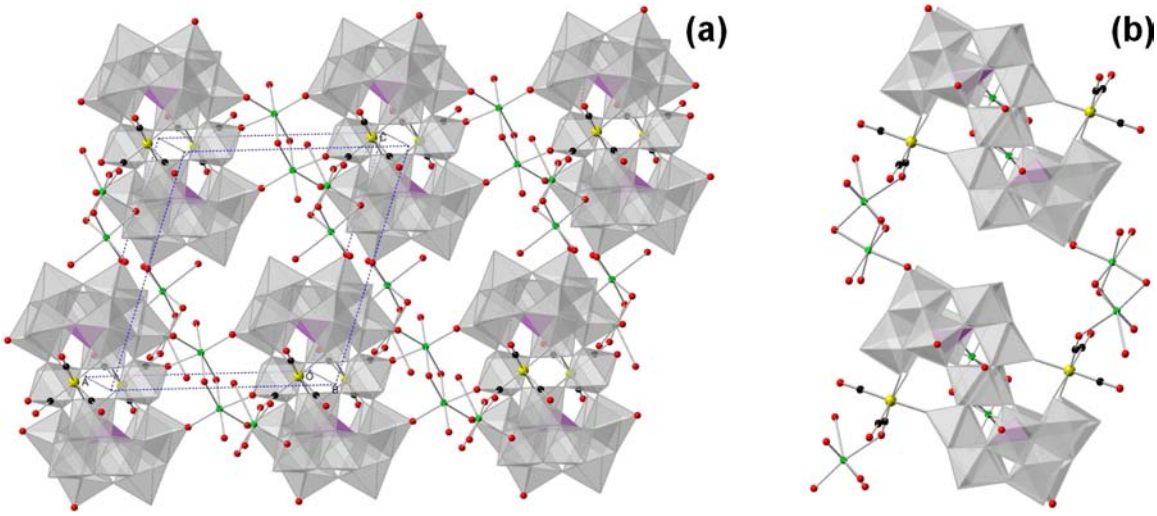

Figure 2. (a) View of the 2D sheet of **1b** in the combined ball-and-stick and polyhedral notation. (b) View of **1b** along the *a*-axis. Na, green; O, red; C, black; Re, yellow; WO_6, gray; SbO_3, purple.

differences in relative bond distances. The MnO_3C_3 moieties, as reflected in M-C distances and M-C-O angle variations, are slightly more distorted from pure octahedral symmetry than the Re derivatives. Typically, the three Re−C bond distances in **1a** and **1b** are almost identical and the Re−C−O angles are nearly 180° (Table 1). The M-C bond distances are 1.87 Å (Re−C) and 1.84 Å (Mn−C) on average, which are similar with those in analogous complexes reported previously.[12,13,15] Compared to **1a** and **1b**, the Mn−C bonds in **2a** and **2b** are more variable, and the Mn−C−O angles are not quite linear (e.g., 171°). Table 2 summarizes the data on these four new POM complexes (both crystallographic and computational).

dx.doi.org/10.1021/ic301766b | *Inorg. Chem.* 2013, 52, 671−678

Furthermore, the polyanions in **1a** are linked by two symmetry-equivalent hydrated Na^+ ions to form a two-dimensional (2D) framework. Along the *a*-axis, the polyanions are connected by dinuclear $\{Na(H_2O)_2\}_2^{2+}$ groups via terminal oxygen atoms on the POM units with Na−O distances of 2.32(2)−2.49(2) Å to form a one-dimensional (1D) chain. The adjacent 1D chains are further bridged through mononuclear $\{Na(H_2O)_2\}^+$ units along the *b*-axis with Na−O (terminal) distances of 2.32(2)−2.35(2) Å to form a 2D network (Figure 1b).

The structure of **1b**, like that of **1a**, consists of a 2D framework where the polyanions are connected by the hydrated Na^+ ions. Along the *a*-axis, a dinuclear unit $\{Na(H_2O)_2\}_2^{2+}$ joins each polyanion to form a 1D chain, as in the structure of **1a**. However, the 1D chains are linked by a dinuclear moiety $[Na_2(H_2O)_7]^{2+}$ via a terminal oxygen on tungsten and a carbonyl group on rhenium along the *b*-axis (forming a Na−O−C−Re linkage) in contrast to the connection in **1a** (Figure 2).

Spectroscopic and Computational Studies of 1a and 1b. The precursors for making **1a** and **1b** are colorless: the POM ligands $[X_2W_{22}O_{74}(OH)_2]^{12-}$ have O(2p) → W(5d) transitions, which absorb significantly only below 300 nm, and the moiety *fac*-$\{Re(CO)_3\}^+$, which has a ligand-to-metal charge-transfer (LMCT) band, only absorbs below 350 nm. In contrast, the UV−vis spectra of **1a** and **1b** show a broad absorption covering the entire UV and visible regions extending to about 600 nm (Figure 3a) with high absorptivity (**1a**: $\varepsilon_{400\ nm}$ about 2400 $M^{-1}\cdot cm^{-1}$; **1b**: about 2100 $M^{-1}\cdot cm^{-1}$). These extinction coefficients are not as high as for the MPCT absorption band in **3** ($\varepsilon_{400\ nm}$ about 6200 $M^{-1}\cdot cm^{-1}$) but are still comparable with the photosensitizer (2,2′-bipyridyl)Re(CO)$_3$Cl (MLCT band; $\varepsilon_{370\ nm}$ about 2500 $M^{-1}\cdot cm^{-1}$ in MeCN).[31−33] On the basis of previous studies, these broad absorptions of **1a** and **1b** in the visible region are likely due to MPCT from the Re centers to POM ligands.[18] Thus **1a** and **1b**, like **3**, are two additional all-inorganic chromophores, that is, they are free of oxidatively and hydrolytically unstable polypyridyl ligands. Furthermore, **1a** and **1b** are very stable in aqueous solutions. The spectra of the stored solutions do not change overnight or after several hours of visible-light (LED; λ = 455 nm) irradiation.

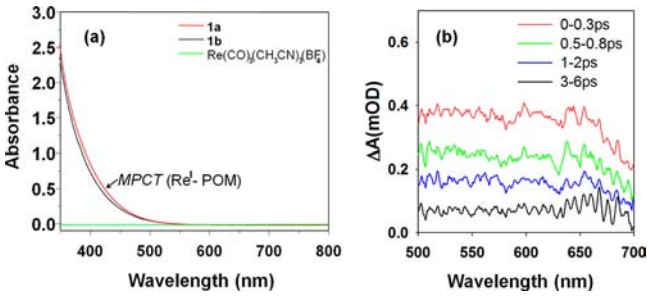

Figure 3. (a) Normalized UV−vis spectra of aqueous **1a** (red), **1b** (black), and $[Re(CO)_3]^+$ (green). (b) Average visible transient absorption spectra of **1a** in H_2O at indicated delay time windows after 400 nm excitation.

The charge transfer dynamics were investigated by femtosecond transient absorption (TA) spectroscopy. As shown in Figure 3b, a broad absorption feature throughout the visible region (500−700 nm) arises after the 400 nm excitation, which is attributed to the W(V) d-d transitions and W(V)−W(VI) intervalence charge transfer (IVCT) transitions in the reduced POM ligands, species historically and currently referred to as "heteropoly blues".[34−39] The kinetics of this photoinduced absorption feature was monitored at 640 nm and fitted by a biexponential function. As shown in Supporting Information, Figure S2 and Table S1, the best fit yields an instantaneous formation within the time resolution of this measurement (about 150 fs), consistent with a metal-to-POM charge transfer (MPCT) transition. However, this CT excited state is still short-lived, with an average lifetime of 1.9 ps, which is similar to that in **3** previously studied.[18] Comparison of the kinetic traces in Supporting Information, Figure S2 indicates that **1b** has very similar charge transfer dynamics to **1a**.

We investigated the origin of the high visible absorptivity of **1a** by computational modeling. Full DFT-optimized geometry parameters of **1a**, in its ground singlet electronic state, are given in Table 1 and in the Supporting Information, Table S2. The frontier molecular orbitals are shown in Figure 4a. As seen in this figure, the two highest occupied orbitals of **1a**, H and H_{-1}, form a near degenerate pair, and each of them has a strong contribution from rhenium d and antimony p orbitals. There is a smaller contribution from the p orbitals of bridging oxygens. The lowest unoccupied orbitals, L and L_{+1}, also form a near degenerate pair. Their character is mainly the d orbitals of the outer W atoms with a small mixture from the p orbitals of associated O atoms. Thus, the $H/H_{-1} \rightarrow L/L_{+1}$ excitations are $[Re(CO)_3 + Sb] \rightarrow$ POM charge transfer excitations. In contrast to the transition in **3**, these computational results indicate that the heteroatom Sb is also involved in the charge-transfer process in **1a**.

The calculated UV−vis spectrum of the singlet excitations is shown in Figure 4b. As expected from the frontier orbital analysis, the first excited state S_1 is a H → L, that is, $[Re(CO)_3 + Sb] \rightarrow$ POM transition occurring at 2.51 eV (492 nm). The following several states are dark until the group of states at about 470 nm, S_8−S_{12}, which are pure Re → POM transitions. Continuing toward the shorter wavelengths, the spectrum begins to be dominated by pure Re → POM transitions, such as those at about 440, 430, and 410 nm, with a few mixed Re/Sb → POM and POM → POM bands (see labeling in Figure 4b; the summary of S_0-S_n transitions is in Supporting Information, Table S3). Thus, the calculated spectrum for compound **1a** is consistent with the experimental result in the visible range (400−600 nm) shown in Figure 3a above.

It should be noted that complex **2a** is found to be less stable at the DFT level of theory (especially at its excited electronic state). Therefore, we were not able to calculate the structure and UV−vis spectrum of this species.

Steady-State Spectroscopy of 2a and 2b. Complexes **2a** and **2b** as solids are dark-red, and their UV−vis spectra in aqueous solution have the characteristic peaks at about 420 nm and a broad absorption up to about 650 nm (Figure 5a). The 420 nm band is attributed to the $[Mn(CO)_3]^+$ unit,[40] and the extended absorption is assigned as a MPCT from the Mn centers to the POM ligands. However, unlike the rhenium compounds (**1a** and **1b**), **2a** and **2b** are fairly stable in the aqueous solution. The solutions slowly become greenish under indoor lighting. This green color indicates that the POM ligands have been reduced (green is a superposition of the yellow oxidized complex with small quantities of the blue reduced complex).[34−39] This observation indicates that the photoinduced charge-transfer from the low-valent Mn centers to the POM ligands is occurring and subsequently results in

dx.doi.org/10.1021/ic301766b | Inorg. Chem. 2013, 52, 671−678

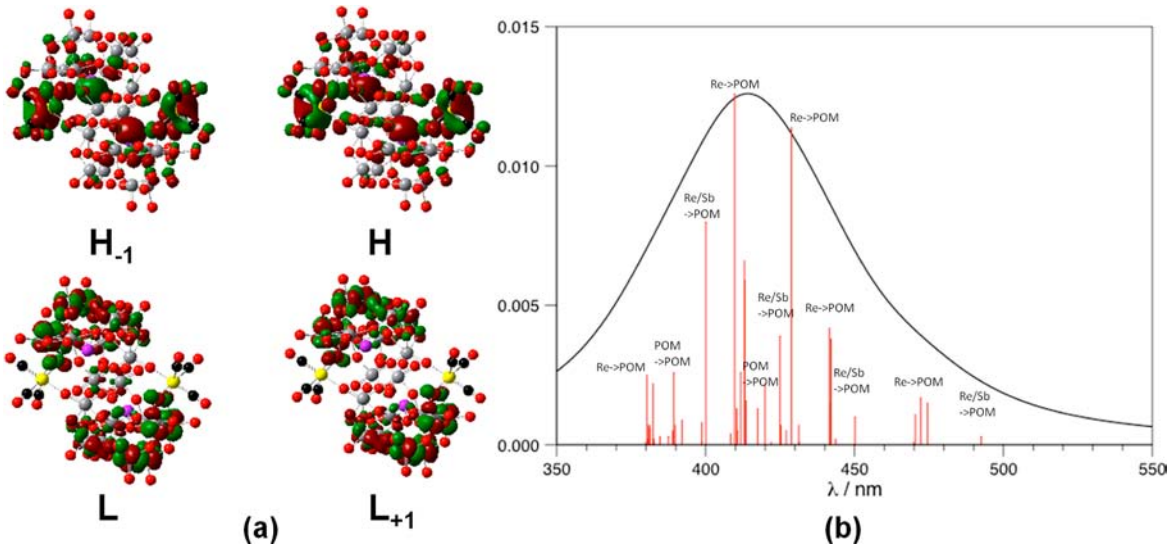

Figure 4. (a) Molecular orbitals and orbital energies (in ascending order −4.82, −4.79, −2.28, −2.25 eV) of S_0 $[Sb_2W_{20}O_{70}\{Re(CO)_3\}_2]^{12-}$ (the polyanion in **1a**) in water. H = HOMO, L = LUMO. Color codes: Re, yellow; W, gray; Sb, purple; O, red; C, black. (b) Calculated UV spectrum of the same polyanion (S_0 state) in water using the first 70 excited singlet states.

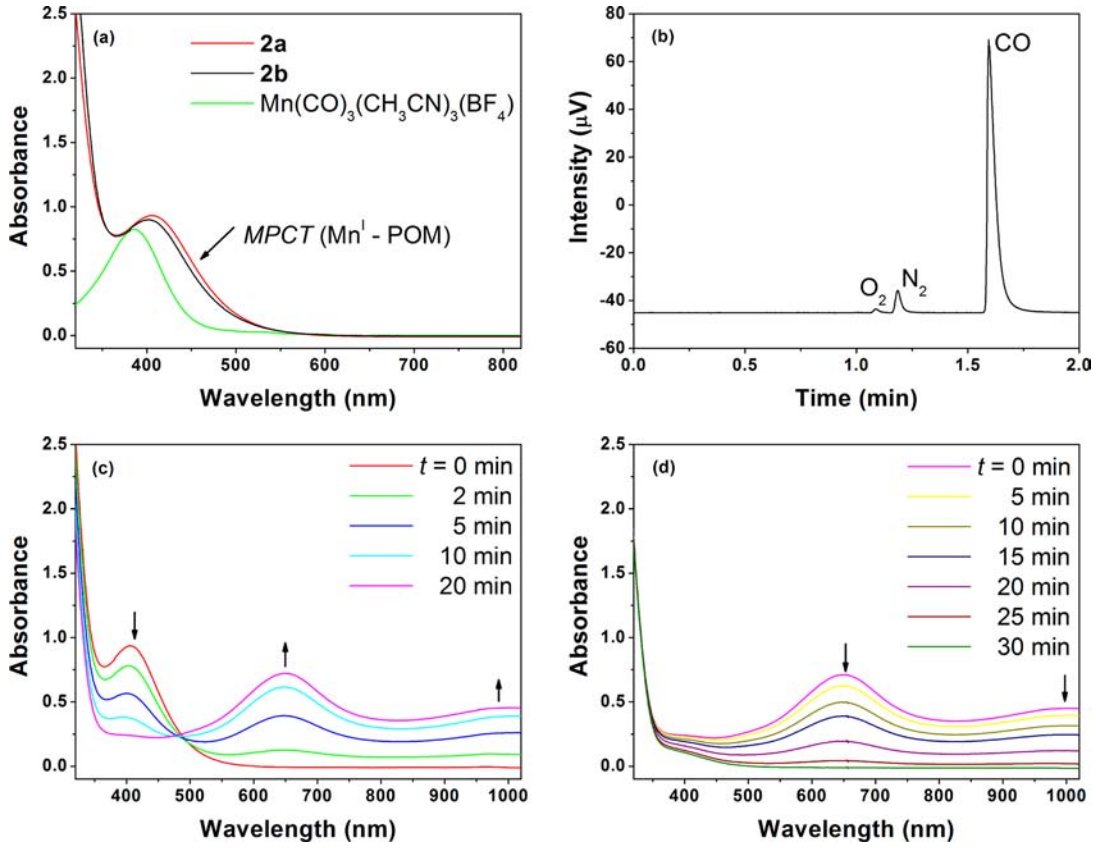

Figure 5. (a) Normalized UV−vis spectra of aqueous **2a**, **2b** and $[Mn(CO)_3]^+$ (2 equiv); (b) GC signals for a gas sample from the head space of a quartz cell containing **2a** after photolysis (deaerated by argon); (c) Time-dependent UV−vis spectra of **2a** in a sealed and deaerated quartz cell exposed to a LED-lamp light (455 nm wavelength, 17mW); (d) Time-dependent UV−vis spectra of the postphotolysis solution of **2a** in the quartz cell exposed to air. Arrows in (c) and (d) indicate the directions of amplitude changes.

decomposition of the starting compounds. This hydrolytic instability likely results in part from photogeneration of d^5 high spin Mn(II) centers which have little or no ligand field stabilization energy and are consequently quite labile.

To monitor the charge-transfer process of **2a** in aqueous solution, a photolysis reaction was performed in a sealed cell deaerated by argon. Upon irradiation (about 20 min), the characteristic band at about 420 nm decreases, new broad absorptions with maximum at about 650 and 1000 nm grow and a point at about 480 nm, which is nearly isosbestic, is observed in the UV−vis spectrum (Figure 5c). These absorption features can be attributed to a bleach of the ground

dx.doi.org/10.1021/ic301766b | *Inorg. Chem.* 2013, 52, 671−678

state absorption and the development of W(V) d-d transitions and W(V)−W(VI) IVCT transitions in the reduced Krebs-type polytungstate ligands, respectively. In addition to producing the "heteropoly blues", CO is detected in the head space gas by GC in about 80% yield (Figure 5b). These results indicate that unlike the fast charge separation and recombination in **1a** and **1b**, the excited electrons in **2a** (located on lowest unoccupied molecular orbital (LUMO) involving the POM ligands) are unable to return to the Mn centers rapidly. The photolysis reaction leads to the dissociation of **2a** which generates the reduced POM ligands and the stoichiometrically oxidized products, Mn^{2+} ions and CO. In the next step, the disappearance of "heteropoly blues" by O_2-based reoxidation is also followed by UV−vis spectra (Figure 5d). The absorptions from about 650 to 1000 nm decrease, and the solution becomes colorless. The absence of the starting characteristic absorption at about 420 nm indicates that the dissociation of **2a** is nearly complete. Similar phenomena are also observed for **2b** (Supporting Information, Figure S3). A possible photolysis pathway based upon the discussion above is shown in Scheme 2.

Scheme 2. Likely Mechanism of the Light-Induced Charge Transfer in 2a and 2b

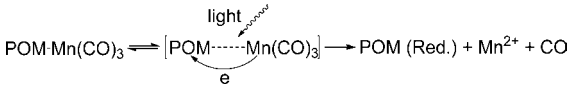

CONCLUSIONS

Four polytungstate-supported tricarbonyl metal derivatives have been synthesized through a facile approach and characterized by X-ray crystallography, spectroscopic methods, transient absorption spectroscopy, and computational studies. These compounds contain very similar geometrical structures: $[XW_9O_{33}(WO_2)\{M(CO)_3\}]_2^{12-}$ (X = Sb, Bi and M = Re, Mn). Notably, **1a** and **1b** show broad absorptions in the visible region attributed to MPCT transitions involving primarily charge transfer from Re to the empty mostly polytungstate-based LUMOs with some involvement of the Sb/Bi heteroatom orbitals in the highest occupied molecular orbitals (HOMOs). Unlike **1a** and **1b**, **2a** and **2b** are unstable upon irradiation. The charge transfer transitions from the Mn centers to the POMs result in decomposition of the starting compounds.

The preparation of these four compounds is performed in aqueous solutions under mild conditions. This synthetic approach is more convenient than reported preparations of similar compounds where organic solvents or one-pot hydrothermal methods are used. This stepwise synthesis indicates that the multidentate multidefect POMs, $[X_2W_{22}O_{74}(OH)_2]^{12-}$ (X = Sb or Bi), are versatile starting materials for construction of functionalized POMs of this type. Together with the previously reported structures by Krebs, the examples in this report suggest that these POM precursors can be further used to coordinate topologically equivalent units, $[LMR_3]^{n+}$ (L = tridentate ligand; M = transition metal; R = weak ligands, such as H_2O, CH_3CN, etc.) that might display chromophoric or catalytic properties of interest.

EXPERIMENTAL SECTION

Materials and Instrumentation. All chemicals were reagent grade and used as supplied. The Sb^{III}/Bi^{III} polyoxometalate precursors $Na_{12}[Sb_2W_{22}O_{74}(OH)_2]\cdot 27H_2O$ and $Na_{12}[Bi_2W_{22}O_{74}(OH)_2]\cdot 44H_2O$ were prepared by literature methods.[29,30] Their purities were determined through FT-IR spectroscopy. The low-valent complexes, $Re(CO)_3(CH_3CN)_3(BF_4)$ and $Mn(CO)_3(CH_3CN)_3(BF_4)$, were made according to the known procedures but using $AgBF_4$ in place of $AgClO_4$.[41] Their purities were analyzed by ^1H NMR and FT-IR spectroscopy.

UV−vis spectra were acquired using an Agilent 8453 spectrophotometer equipped with a diode-array detector and an Agilent 89090A cell temperature controller unit. The FT-IR spectra were measured on a Thermo Nicolet 6700 spectrometer with KBr pellets (2%). Elemental analyses (Bi, K, Mn, Na, Sb, Re, W) were performed by Galbraith Lab Inc., Knoxville, TN, 37921. Thermogravimetric analysis was acquired on a Perkin-Elmer STA 6000 analyzer.

$Na_{11}H[Sb_2W_{20}O_{70}\{Re(CO)_3\}_2]\cdot 34H_2O$ (1a). $Na_{12}[Sb_2W_{22}O_{74}(OH)_2]\cdot 27H_2O$ (0.1 mmol, 670 mg) and $Re(CO)_3(CH_3CN)_3(BF_4)$ (0.2 mmol, 98 mg) were dissolved in 20 mL of H_2O. The mixture was heated at about 70 °C for 30 min, and the color changed to orange. NaCl (400 mg) was added to the solution, and the pH was adjusted to 5 by addition of 1 M NaOH. The solution was cooled to room temperature and then filtered. The solution was allowed to stand out at room temperature for about a week at which point large orange block-shaped crystals were obtained. Yield: 150 mg (22% based on Sb). FTIR (2% KBr pellet, 2500−400 cm^{-1}): 2016 (s), 1925 (s), 1906 (s), 955 (s), 836 (m), 808 (s), 767 (m), 657 (m), 472 (sh). Electronic spectral data (300−800 nm, in H_2O): $\varepsilon_{400\ nm}$ about 2200 M^{-1} cm^{-1}. Anal. Calcd. for $C_6H_{69}O_{110}Na_{11}Re_2Sb_2W_{20}$: Na, 3.9; Re, 5.8; Sb, 3.8; W, 57.0. Found: Na, 4.0; Re, 5.3; Sb, 3.3; W, 55.4. Thermogravimetric analysis (TGA; 30−500 °C): weight loss, 12.1%.

$Na_{11}H[Bi_2W_{20}O_{70}\{Re(CO)_3\}_2]\cdot 33H_2O$ (1b). This compound was prepared using a similar procedure to **1a** except that $Na_{12}[Bi_2W_{22}O_{74}(OH)_2]\cdot 44H_2O$ was used as the POM ligand precursor. Orange-red crystals were obtained after several days of evaporation. Yield: 130 mg (20% based on Bi). FTIR (2% KBr pellet, 2500−400 cm^{-1}): 2014 (s), 1923 (s), 1900 (s), 945 (s), 837 (sh), 798 (s), 765 (m), 646 (m), 459 (sh). Electronic spectral data (300−800 nm, in H_2O): $\varepsilon_{400\ nm}$ about 2100 M^{-1} cm^{-1}. Anal. Calcd. for $C_6H_{67}O_{109}Bi_2Na_{11}Re_2W_{20}$: Bi, 6.3; Na, 3.8; Re, 5.6; W, 55.7. Found: Bi, 6.5; Na, 3.8; Re, 5.3; W, 55.7. Thermogravimetric analysis (TGA; 30−500 °C): weight loss, 11.5%.

$K_9Na_3[Sb_2W_{20}O_{70}\{Mn(CO)_3\}_2]\cdot 32H_2O$ (2a). $Na_{12}[Sb_2W_{22}O_{74}(OH)_2]\cdot 27H_2O$ (0.1 mmol, 670 mg) was dissolved in 20 mL of H_2O, then excess $Mn(CO)_3(CH_3CN)_3(BF_4)$ (0.25 mmol, 88 mg) in 2 mL of CH_3OH was added slowly. The reaction beaker was covered with aluminum foil. The mixture was stirred for 30 min in dark, and the pH was adjusted to 6.0 by 0.1 M KOH. KCl (0.5 mL of a 1.0 M solution) was then added to the mixture. The solution was quickly passed through a filter paper and kept in the dark. Dark-red crystals in plate-shape were collected after 2 weeks. Yield: 120 mg (20% based on Sb). FTIR (2% KBr pellet, 2500−400 cm^{-1}): 2031 (s), 1936 (s), 1919 (s), 946 (s), 838 (m), 806 (m), 768 (m), 667 (w), 455 (sh). Electronic spectral data (300−800 nm, in H_2O): $\varepsilon_{400\ nm}$ about 3500 M^{-1} cm^{-1}. Anal. Calcd. for $C_6H_{64}O_{108}Mn_2K_9Na_3Sb_2W_{20}$: K, 5.6; Mn, 1.7; Na, 1.1; Sb, 3.9; W, 58.2. Found: K, 6.0; Mn, 1.7; Na, 1.1; Sb, 3.5; W, 60.7. Thermogravimetric analysis (TGA; 30−500 °C): weight loss, 11.8%.

$K_9Na_3[Bi_2W_{20}O_{70}\{Mn(CO)_3\}_2]\cdot 32H_2O$ (2b). This compound was made by a similar procedure as **2a**. Yield: 100 mg (18% based on Bi). FTIR (2% KBr pellet, 2500−400 cm^{-1}): 2030 (s), 1935 (s), 1919 (s), 941 (s), 826 (m), 797 (m), 760 (m), 651 (w), 409 (sh). Electronic spectral data (300−800 nm, in H_2O): $\varepsilon_{400\ nm}$ about 3400 M^{-1} cm^{-1}. Anal. Calcd. for $C_6H_{64}O_{110}K_9Na_3Mn_2Bi_2W_{20}$: Bi, 6.4; K, 5.4; Mn, 1.7; Na, 1.1; W, 56.7. Found: Bi, 6.1; K, 5.6; Mn, 1.8; Na, 1.2; W, 56.8. Thermogravimetric analysis (TGA; 30−500 °C): weight loss, 11.4%.

Crystallography. X-ray analysis was performed on a Bruker D8 SMART APEX CCD sealed tube diffractometer at Emory University. Diffraction intensities were measured using graphite monochromated Mo Kα radiation (λ = 0.71073 Å) at 173(2) K. Data collection, indexing, and initial cell refinements were carried out by using SMART;[42] frame integration and final cell refinements were done by SAINT.[43] A multiple absorption correction including face-indexing

dx.doi.org/10.1021/ic301766b | Inorg. Chem. 2013, 52, 671−678

was done by the program SADABS.[44] The molecular structures of **1a**, **1b**, **2a**, and **2b** were determined by Direct Methods and Fourier techniques and refined by full-matrix least-squares. Structure solution, refinement, graphic and generation of publication materials were accomplished using SHELXTL-97 software.[45,46] The largest residual electron density for each structure was located close to the Sb, Bi, and W atoms and was most likely due to imperfect absorption corrections frequently encountered in heavy-metal atom structures. Crystal data collection and refinement parameters are given in Table 2. Complete details can be found in the .cif files in the Supporting Information.

Computational Details. Geometries of the polyanion **1a** were optimized in implicit water solution, with no geometry constraints, in its ground singlet (S_0) state. Vibrational analyses were performed to ensure that all converged structures are true minima. In these calculations we used the DFT method (M06L functional)[47] in conjunction with the split-valence 6-31G(d) basis sets for C, O and lanl2dz basis sets and associated effective core potentials (ECPs)[48−50] for the W, Sb, and Re atoms, which below are referred to as M06L/[lanl2dz +6-31G(d,p)]. The solvent effects were approximated by the polarizable continuum model (PCM)[51,52] employing the UFF[53] radii for all atoms. Electronic spectra and electric dipole transition moments for S_0-S_n transitions were calculated at the optimized geometries of S_0 of the corresponding compound using the time-dependent (TD)[54] DFT [i.e., TD-M06L/[lanl2dz +6-31G(d)] approach. The total number of states in TD-DFT was chosen based on the short wavelength limit in the experimental spectra. We found that 70 excited states reached far enough into the UV range to provide a good comparison with experiment. The above calculations were carried out with Gaussian 09 software package.[55]

■ ASSOCIATED CONTENT

Ⓢ Supporting Information

X-ray crystallographic files in CIF format, full DFT-optimized geometry parameters of **1a**, in its ground singlet electronic state, FTIR spectra and additional steady-state and ultrafast spectroscopic spectra. This material is available free of charge via the Internet at http://pubs.acs.org.

■ AUTHOR INFORMATION

Corresponding Author

*E-mail: chill@emory.edu.

Notes

The authors declare no competing financial interest.

■ ACKNOWLEDGMENTS

We thank Dr. Yurii Geletii for general discussion and Dr. John Bacsa for the assistance on the X-ray crystal structure determination. We thank the National Science Foundation, Grant CHE-0911610, for support. The authors gratefully acknowledge NSF instrumentation MRI-R2 grant (CHE-0958205) and the use of the resources of the Cherry Emerson Center for Scientific Computation.

■ REFERENCES

(1) Kulkarni, A.; Lobo-Lapidus, R. J.; Gates, B. C. *Chem. Commun.* **2010**, *46*, 5997.
(2) *Special Thematic Issue on Polyoxometalates*; Hill, C. L., Ed.; *Chem. Rev.* **1998**; Vol. *98*, No. 1.
(3) Gouzerh, P.; Proust, A. *Chem. Rev.* **1998**, *98*, 77.
(4) Besecker, C. J.; Klemperer, W. G. *J. Am. Chem. Soc.* **1980**, *25*, 7598.
(5) Day, V. W.; Fredrich, M. F.; Thompson, M. R.; Klemperer, W. G.; Liu, R. S.; Shum, W. *J. Am. Chem. Soc.* **1981**, *103*, 3597.
(6) Besecker, C. J.; Day, V. W.; Klemperer, W. G.; Thompson, M. R. *Inorg. Chem.* **1985**, *24*, 44.
(7) Klemperer, W. G.; Main, D. J. *Inorg. Chem.* **1990**, *29*, 2355.
(8) Klemperer, W. G.; Zhong, B. X. *Inorg. Chem.* **1993**, *32*, 5821.
(9) Siedle, A. R.; Lyon, P. A.; Hodgson, K. O.; Roe, A. L. *Inorg. Chem.* **1987**, *26*, 219.
(10) Nagata, T.; Pohl, B. M.; Weiner, H.; Finke, R. G. *Inorg. Chem.* **1997**, *36*, 1366.
(11) Besserguenev, A. V.; Dickman, M. H.; Pope, M. T. *Inorg. Chem.* **2001**, *40*, 2582.
(12) Villanneau, R.; Delmont, R.; Proust, A.; Gouzerh, P. *Chem.—Eur. J.* **2000**, *6*, 1184.
(13) Villanneau, R.; Proust, A.; Robert, F.; Gouzerh, P. *Chem.—Eur. J.* **2003**, *9*, 1982.
(14) Sadakane, M.; Iimuro, Y.; Tsukuma, D.; Bassil, B. S.; Dickman, M. H.; Kortz, U.; Zhang, Y.; Ye, S.; Ueda, W. *Dalton Trans.* **2008**, 6692.
(15) Niu, J.; Yang, L.; Zhao, J.; Ma, P.; Wang, J. *Dalton Trans.* **2011**, *40*, 8298.
(16) Zhao, J.; Wang, J.; Zhao, J.; Ma, P.; Wang, J.; Niu, J. *Dalton Trans.* **2012**, *41*, 5832.
(17) Zhao, J.; Zhao, J.; Ma, P.; Wang, J.; Niu, J.; Wang, J. *J. Mol. Struct.* **2012**, *1019*, 61.
(18) Zhao, C.; Huang, Z.; Rodríguez-Córdoba, W.; Kambara, C. S.; O'Halloran, K. P.; Hardcastle, K. I.; Musaev, D. G.; Lian, T.; Hill, C. L. *J. Am. Chem. Soc.* **2011**, *133*, 20134.
(19) Hawecker, J.; Lehn, J.-M.; Ziessel, R. *J. Chem. Soc., Chem. Commun.* **1983**, 536.
(20) Takeda, H.; Koike, K.; Inoue, H.; Ishitani, O. *J. Am. Chem. Soc.* **2008**, *130*, 2023.
(21) Takeda, H.; Ishitani, O. *Coord. Chem. Rev.* **2010**, *254*, 346.
(22) Kumar, B.; Smieja, J. M.; Kubiak, C. P. *J. Phys. Chem. C* **2010**, *114*, 14220.
(23) Benson, E. E.; Kubiak, C. P.; Sathrum, A. J.; Smieja, J. M. *Chem. Soc. Rev.* **2009**, *38*, 89.
(24) Long, D.-L.; Tsunashima, R.; Cronin, L. *Angew. Chem., Int. Ed.* **2010**, *49*, 1736.
(25) Long, D.-L.; Burkholder, E.; Cronin, L. *Chem. Soc. Rev.* **2007**, *36*, 105.
(26) Kikukawa, Y.; Yamaguchi, K.; Mizuno, N. *Inorg. Chem.* **2010**, *49*, 8194.
(27) Zhu, G.; Geletii, Y. V.; Zhao, C.; Musaev, D. G.; Song, J.; Hill, C. L. *Dalton Trans.* **2012**, *41*, 9908.
(28) Proust, A.; Matt, B.; Villanneau, R.; Guillemot, G.; Gouzerh, P.; Izzet, G. *Chem. Soc. Rev.* **2012**, *41*, 7605−7622.
(29) Bosing, M.; Loose, I.; Pohlmann, H.; Krebs, B. *Chem.—Eur. J.* **1997**, *3*, 1232.
(30) Loose, I.; Droste, E.; Boesing, M.; Pohlmann, H.; Dickman, M. H.; Rosu, C.; Pope, M. T.; Krebs, B. *Inorg. Chem.* **1999**, *38*, 2688.
(31) Kalyanasundaram, K. *J. Chem. Soc., Faraday Trans. 2* **1986**, *82*, 2401.
(32) Worl, L. A.; Duesing, R.; Chen, P.; Ciana, L. D.; Meyer, T. J. *J. Chem. Soc., Dalton Trans.* **1991**, 849.
(33) Ziessel, R.; Juris, A.; Venturi, M. *Inorg. Chem.* **1998**, *37*, 5061.
(34) Sanchez, C.; Livage, J.; Launay, J. P.; Fournier, M.; Jeannin, Y. *J. Am. Chem. Soc.* **1982**, *104*, 3194.
(35) Sanchez, C.; Livage, J.; Launay, J. P.; Fournier, M. *J. Am. Chem. Soc.* **1983**, *105*, 6817.
(36) Buckley, R. I.; Clark, R. J. H. *Coord. Chem. Rev.* **1985**, *65*, 167.
(37) Kozik, M.; Hammer, C. F.; Baker, L. C. W. *J. Am. Chem. Soc.* **1986**, *108*, 7627.
(38) Papaconstantinou, E. *Chem. Soc. Rev.* **1989**, *18*, 1.
(39) Chiang, M.-H.; Soderholm, L.; Antonio, M. R. *Eur. J. Inorg. Chem.* **2003**, *2003*, 2929.
(40) Bamford, C. H.; Coldbeck, M. *J. Chem. Soc., Dalton Trans.* **1978**, 4.
(41) Edwards, D. A.; Marshalsea, J. *J. Organomet. Chem.* **1977**, *131*, 73.
(42) *SMART*; Bruker AXS: Madison, WI, 2003.
(43) *SAINT*; Bruker AXS: Madison, WI, 2003.
(44) Sheldrick, G. *SADABS*, ver. 2.10.; University of Göttingen: Göttingen, Germany, 2003.

(45) Sheldrick, G. M. *Acta Crystallogr., Sect. A* **1990**, *46*, 467.
(46) Sheldrick, G. M. *SHELXL-97, Program for the Refinement of Crystal Structures*; University of Göttingen: Göttingen, Germany, 1997.
(47) Zhao, Y.; Truhlar, D. G. *Theor. Chem. Acc.* **2008**, *120*, 215.
(48) Hay, P. J.; Wadt, W. R. *J. Chem. Phys.* **1985**, *82*, 270.
(49) Hay, P. J.; Wadt, W. R. *J. Chem. Phys.* **1985**, *82*, 299.
(50) Wadt, W. R.; Hay, P. J. *J. Chem. Phys.* **1985**, *82*, 284.
(51) Tomasi, J.; Persico, M. *Chem. Rev.* **1994**, 2027.
(52) Cammi, R.; Tomasi, J. *J. Comput. Chem.* **1995**, *16*, 1449.
(53) Rappe, A. K.; Casewit, C. J.; Colwell, K. S.; Goddard, W. A.; Skiff, W. M. *J. Am. Chem. Soc.* **1992**, *114*, 10024.
(54) Bauerschmitt, R.; Ahlrichs, R. *Chem. Phys. Lett.* **1996**, *256*, 454.
(55) Frisch, M. J. et al. *Gaussian 09*, revision A.1; Gaussian, Inc.: Wallingford, CT, 2009.